ISIJ International, Vol. 42 (2002), No. 5, pp. 520–526

A Three Dimensional Modified Cellular Automaton Model for the Prediction of Solidification Microstructures

M. F. ZHU and C. P. HONG[1)]

Center for Computer-Aided Materials Processing (CAMP), Department of Metallurgical Engineering, Yonsei University, Shinchon-dong, Seodaemun-ku, Seoul 120-749 Korea, also at Department of Mechanical Engineering, Southeast University, Nanjing, P.R.China. 1) Center for Computer-Aided Materials Processing (CAMP), Department of Metallurgical Engineering, Yonsei University, Shinchon-dong, Seodaemun-ku, Seoul 120-749 Korea. E-mail: hong@yonsei.ac.kr

(*Received on December 17, 2001; accepted in final form on February 6, 2002*)

A three dimensional modified cellular automaton model (3-D MCA) was developed in order to simulate the evolution of microstructures in solidification of alloys. Different from the classical cellular automata in which only the temperature field was calculated, this model included the solute redistribution both in liquid and solid during solidification. The relationship between the growth velocity of a dendrite tip and the local undercooling, which consists of thermal, constitutional and curvature undercooling terms, was calculated according to the KGT (Kurz–Giovanola–Trivedi) and LKT (Lipton–Kurz–Trivedi) models. The finite volume method, which was coupled with the cellular automaton model, was used to calculate the temperature and solute fields in the calculation domain. The present 3-D MCA model was applied to predict the microstructures, such as the free dendritic growth from an undercooled melt, the competitive dendritic growth in practical casting solidification. Some of the simulated results were compared with those obtained experimentally.

KEY WORDS: solidification; microstructure simulation; cellular automaton; nucleation; growth kinetics; solute redistribution; diffusion; curvature; finite volume method.

1. Introduction

Mechanical properties of casting products are closely associated with their solidification microstructures. It is therefore very important to control solidification microstructures to obtain high quality products in practical casting processes. Over the last decade, significant advances have been made in the fundamental understanding of microstructure evolution in solidification of alloys. In parallel to the development of rigorous analytical models and more refined experimental techniques, numerical modeling has presented its considerable potential for quantitatively understanding the solidification microstructure evolution.[1)] With the development of powerful computers and advanced numerical techniques, it is possible to analyse transport phenomena including heat, mass and fluid flow in the mushy zone to a high level of details.[2)]

Coupling of the macroscopic heat transfer analysis and the microscopic modeling of solidification has been recently focused on in order to predict solidification structures. A series of studies, applying the two-dimensional and three-dimensional cellular automaton models coupled with the finite volume method (CA-FVM) or finite element method (CAFE) for the macroscopic heat flow calculation, have been reported to simulate the solidification grain structures formed in various casting processes.[3–16)]

However, it is well known that the classical CA models mentioned above have the limitation that they are unable to describe the detailed microstructure evolution including the dendritic side branching and the formation of second phases (eutectic). This limitation has been solved by a two-dimensional modified cellular automaton (2-D MCA) model which has been recently developed by the authors.[17)] The MCA model can quantitatively describe the evolution of dendritic growth features, including the growing and coarsening of the primary trunks, the branching of the secondary and tertiary dendrite arms, as well as the solute segregation patterns. The MCA model can successfully predict multi-dendritic growth in solidification of alloys and can also be used for the prediction of non-dendritic or globular structure evolution in the semi-solid casting process.[18)] It was found that the newly developed 2-D MCA model is able to bridge the gap between the phase field models, which are in the microscopic scale and presently limited to a very small calculation domain,[19–24)] and the classical CA models which are limited to simulate the macroscopic grain structures.

The aim of the present study is to extend the 2-D MCA model into the three dimensional model in order to simulate three-dimensional microstructure evolution in solidification of alloys. Different from the classical cellular automaton models in which only the temperature field is calculated, the present model includes the curvature effect and the solute redistribution in the liquid and solid phases during solidification. The present model was applied to simulate the three dimensional microstructure evolution in solidification of alloys for various casting processes. Some of the simulated results were compared with those obtained experimentally.

2. Model Description

2.1. The Stochastic Cellular Automaton

A cellular automaton is a mathematical idealization of physical systems in which space and time are discrete, and physical quantities take on a finite set of discrete values.[25] In this work, the calculation domain is divided into uniform cubic cells in the three dimensions. Each cell is characterized by different variables (such as temperature, concentration, crystallographic orientation and solid fraction) and states (solid or liquid). The definition of neighborhood includes the 26 surrounding neighbor cells of the first layer. The cellular automaton evolves in discrete time step, and the state of a cell at a particular time is calculated from the local rule, such as the nucleation and growth kinetics. Similar with other CA models, the present model uses a deterministic growth algorithm, but the location and crystallographic orientation of nuclei are randomly chosen.

2.2. Nucleation and Growth Kinetics

Nucleation conditions are very important in determining the characteristics of microstructures. The number, shape and size of grains vary according to the solidification conditions. In the present study, the continuous nucleation model was adopted for describing the heterogeneous nucleation both on the mold wall and in the bulk liquid. The grain density increase d_n is induced by an increase in the undercooling $d(\Delta T)$ according to the Gaussian distribution,[17,26] which is characterized by the mean nucleation undercooling ΔT_{mn}, the standard deviation ΔT_σ and the maximum density of nuclei n_{max}.

The characteristics of dendritic growth can be represented by two analytical models, the KGT (Kurz–Giovanola–Trivedi) model[27] and the LKT (Lipton–Kurz–Trivedi) model.[28] In the KGT model, the constrained dendritic growth is considered with a positive temperature gradient in the liquid at the solid/liquid (S/L) interface. On the other hand, the LKT model describes the dendritic growth into an undercooled melt in which the thermal gradient in the liquid at the S/L interface is assumed negative. In many rapid solidification processes, such as splat cooling on a substrate, melt spinning and atomization, the existence of negative undercooling in the liquid ahead of the S/L interface has been demonstrated both by experiments and heat transfer analyses.[29] In the present simulation, the growth velocity of a dendrite tip was calculated by the KGT model for normal solidification condition and by the LKT model for gas atomization.

2.3. Solute Redistribution

The assumptions used for solute redistribution are as follows:

(1) The local equilibrium at the S/L interface is preserved as follow.

$$C_s^* = kC_l^* \quad \text{.....(1)}$$

where k is the partition coefficient, C_s^* and C_l^* are the interface equilibrium concentrations in the solid and liquid phases, respectively.

(2) The solute field during solidification is mainly controlled by diffusion in liquid and solid, and no consideration on convective mass transfer is made.

As the solidification proceeds, the solidified cell rejects solute to its neighbor liquid cells. The governing equation for the solute redistribution in the liquid region is given by

$$\frac{\partial C}{\partial t} = D_l \cdot \nabla^2 C + C(1-k)\frac{\partial f_s}{\partial t} \quad \text{.....(2)}$$

where t is the time, D_l is the solute diffusion coefficient in the liquid phase, f_s is the solid fraction, and k is the partition coefficient. The last term on the right hand side of the Eq. (2) indicates the amount of solute rejected at the S/L interface.

The governing equation for diffusion in solid phase is given by

$$\frac{\partial C}{\partial t} = D_s \cdot \nabla^2 C \quad \text{.....(3)}$$

where D_s is the solute diffusion coefficient in the solid phase.

2.4. Macroscopic Thermal Transport

In order to verify the present model, three cases were examined: i) isothermal dendritic growth from an undercooled melt; ii) directional solidification and iii) dendritic growth of atomized droplets.

The finite volume method was used to calculate three-dimensional transient heat transfer in directional solidification and gas atomization processes. The governing equation is given by

$$\rho C_p \frac{\partial T}{\partial t} = \lambda \cdot \nabla^2 T + \rho \Delta H \frac{\partial f_s}{\partial t} \quad \text{.....(4)}$$

where T is temperature, ρ is the density, C_p is the specific heat, λ is the thermal conductivity, f_s is the solid fraction and ΔH is the latent heat of freezing, respectively.

The boundary conditions at the melt/mold interface and droplet/atmosphere could be found elsewhere.[11,17]

3. Numerical Method

3.1. Nucleation and Growth Algorithm

Heterogeneous nuclei formed on the mold wall or in the bulk liquid were assumed to have random crystallographic orientations. The preferential growth orientation corresponds to ⟨100⟩ for cubic metals in the present three-dimensional model. At the beginning of simulation, nucleation sites are randomly set according to Gaussian distribution,[17,26] and each nucleation site is identified with reference integer that is related to a corresponding undercooling for nucleation. During a time step interval, if a given cell is a predetermined nucleation site and the local undercooling is larger than that which is necessary for nucleation, this cell changes its state from liquid to solid. At the same time, the preferential growth orientation of a new crystal is determined by a random process. In the present study, each possible growth orientation is constructed by three Euler angles. As shown in **Fig. 1**(a), the orientation of the [001] dendrite arm can be characterized by two Euler angles, ϕ and θ. The values of ϕ and θ are in the ranges of $\phi(-\pi, \pi)$ and $\theta(0, \pi/2)$, respectively. The third Euler angle φ, characterizing the spin of the [001] dendrite arm, is in the range of $\varphi(-\pi/4, \pi/4)$. Figure 1(b) indicates the definition of a crys-

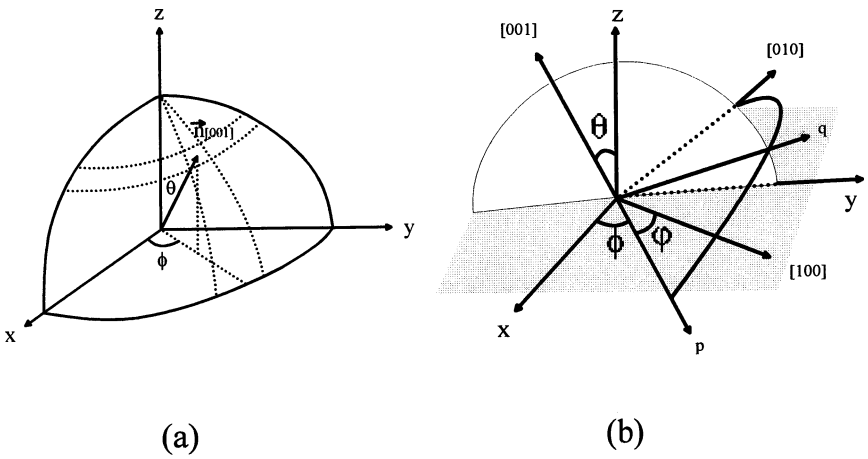

Fig. 1. Crystallographic orientation of a nucleus: (a) the definition of the first and second Euler angles, ϕ and θ; and (b) crystallographic orientation defined by three Euler angles.

tallographic orientation by three Euler angles. The detailed procedure of randomly determining three Euler angles for the possible orientation could be found elsewhere.[11)]

Once a cell has nucleated, it will grow with a preferential direction corresponding to its crystallographic orientation having a growth velocity determined by the local undercooling. Let us consider a solidified cell labeled "A" which lies at the S/L interface, as shown in **Fig. 2**. There must exist at least one liquid cell within its 26 surrounding neighbors. Figure 2 describes the details of the growth algorithm between the solid cell A and its liquid neighbor cell i. The $l_A^i(t_n)$ in Fig. 2 is the growth length of the solid cell A respecting to its liquid neighbor cell i at time t_n, which can be calculated by

$$l_A^i(t_n) = W_A^i \cdot \sum_{n=1}^{N} [v_n\{\Delta T(t_n)\} \times \Delta t_n] \quad \text{.....(5)}$$

where Δt_n is the time step and N indicates the iteration number. W_A^i is the orientation weight coefficient related to the angle between the cell A's preferential growth direction and vector $\vec{L}_A^i$. As shown in Fig. 2, $\vec{L}_A^i$ indicates the vector from the cell A linking to its neighbor cell i. The orientation weight coefficient W_A^i is given by

$$W_A^i = \mathrm{Max}[|X_w|, |Y_w|, |Z_w|] \quad \text{.....(6)}$$

here X_w, Y_w and Z_w can be calculated by

$$\begin{bmatrix} X_w \\ Y_w \\ Z_w \end{bmatrix} = \begin{bmatrix} x_p & x_q & x_r \\ y_p & y_q & y_r \\ z_p & z_q & z_r \end{bmatrix} \cdot \begin{bmatrix} p_A^i \\ q_A^i \\ r_A^i \end{bmatrix} \quad \text{.....(7)}$$

where (x_p, x_q, x_r), (y_p, y_q, y_r) and (z_p, z_p, z_r) are the direction cosines of the [100], [010] and [001] dendrite arms relating to the coordinate x, y and z axes, respectively. (p_A^i, q_A^i, r_A^i) are the direction cosines of the vector $\vec{L}_A^i$, relating to the coordinate x, y and z axes.

$v_n\{\Delta T(t_n)\}$ in Eq. (5) is the growth rate, which can be calculated using the KGT or the LKT model depending upon the local undercooling, $\Delta T(t_n)$, taken at the center of the cell i. In the present simulation, the relationships between the

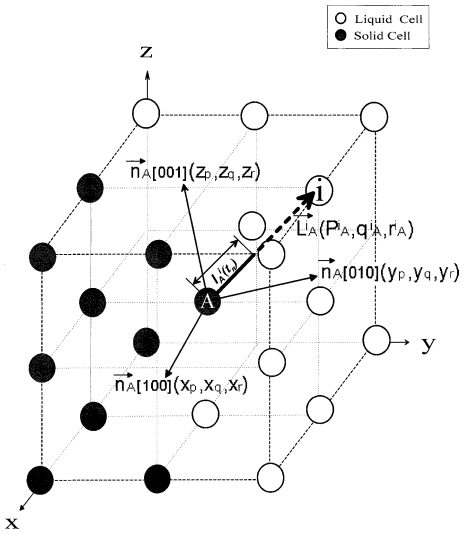

Fig. 2. A schematic diagram of the growth algorithm used in the 3-D MCA model.

growth velocity and the local undercooling for Al–Cu alloys are taken from the literatures.[10,11)] The present model takes account of the contributions associated with thermal, solutal and curvature undercoolings. Therefore, the local undercoling $\Delta T(t_n)$ is given by

$$\Delta T(t_n) = T_1 - T_i(t_n) + m \cdot (C_i(t_n) - C_0) - \Gamma \bar{K}_i(t_n) \quad \text{..... (8)}$$

where T_1 is the equilibrium liquidus temperature, m the liquidus slope, C_0 the initial concentration and Γ the Gibbs–Thomson coefficient. $\bar{K}_i(t_n)$, $C_i(t_n)$ and $T_i(t_n)$ are the mean curvature, the concentration and the temperature of the cell i on the S/L interface at time t_n, respectively. Then, the solid fraction of the cell i at a certain time $f_s^i(t_n)$ can be expressed by

$$f_s^i(t_n) = \frac{l_A^i(t_n)}{L_A^i} \quad \text{.....(9)}$$

where L_A^i is the spacing between the cell A and the cell i, as shown in Fig. 2: if i is one of the six nearest neighbors, $L_A^i = dx$; if i is one of the twelve second-nearest neighbors, $L_A^i = \sqrt{2}dx$; and if i is the one of the eight third-nearest neighbors, $L_A^i = \sqrt{3}dx$. When $f_s^i(t_n) \geq 1$, which means that the

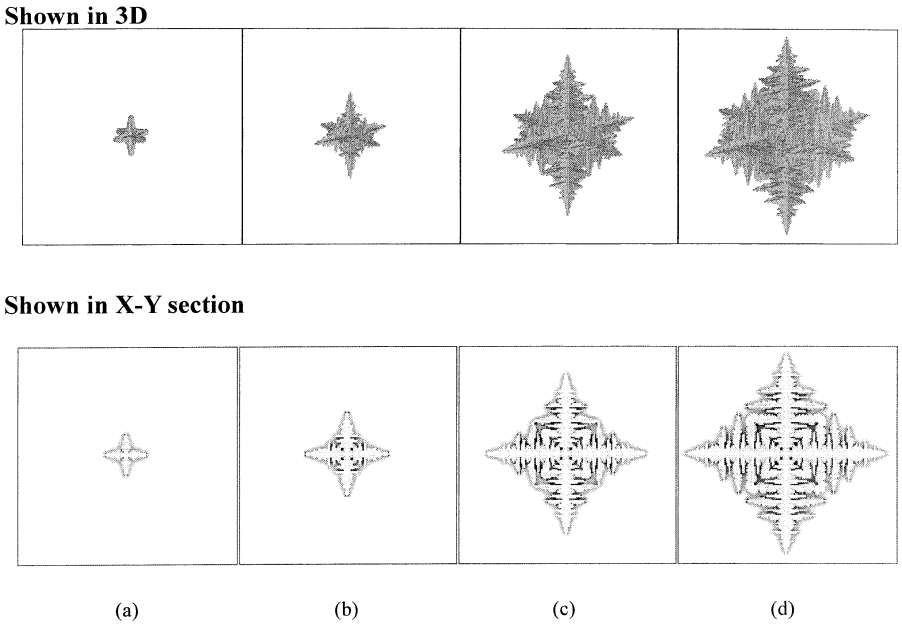

Fig. 3. Growth sequence of a 3-D dendrite during isothermal growth of an Al–15mass%Cu alloy at 878 K (ΔT=10 K) for various growth time: (a) 0.016 s, (b) 0.03 s, (c) 0.045 s and (d) 0.06 s. The calculation domain was divided into 160×160×160 cubic cells and the cell size was 1 μm.

growth front of the solid cell A can touch the center of the liquid cell i, the cell i will then transform its state from liquid to solid and get the same orientation index as the cell A.

By means of the algorithm described above, the primary dendrite will grow and coarsen with the preferential ⟨100⟩ direction. As the growing and the coarsening of a primary trunk proceed, the solute will be enriched in the liquid near the S/L interface due to the solute redistribution, which will destroy the interface stability and therefore cause the side branching of dendrite arms.

3.2. Calculation of the Interface Curvature

The interface curvature in a cell with a solid fraction f_s for the 3-D model is calculated in the same way as in the 2-D MCA model.[17,30] In the present 3-D model, the number of the neighboring cells is equal to 26, which includes the surrounding neighbor cells of the first layer. The values of the curvature vary from $1/dx$ to 0 for convex surface and from 0 to $-1/dx$ for concave surface.

3.3. Calculation of the Concentration and Temperature Fields

When a cell transforms its state from liquid to solid by nucleation or growth, its concentration will be changed according to Eq. (1). Consequently, this cell will liberate the amount of solute, $dC=C_l^*-kC_l^*$, which is assumed to be distributed to its liquid neighbor cells. An explicit finite difference scheme was applied for calculating the solute diffusion in both the solid and liquid phases using Eqs. (2) and (3), and transient heat transfer using Eq. (4). The thermal and physical properties used in the present calculation were taken from literature.[17]

4. Results and Discussion

4.1. Free Dendritic Growth in an Undercooled Melt

In order to simulate free dendritic growth into an undercooled melt, the calculation domain is divided into 160×160×160 cubic cells with a cell size of 1 μm. In the beginning of simulation, one nucleus with the crystallographic orientation of three zero Euler angles, ϕ=0°, θ=0° and φ=0°, was assigned in the center of the area.

The simulated dendrite morphology of an Al–15mass% Cu alloy solidified into an undercooled melt (ΔT=10 K) is shown in **Fig. 3**. The figures on the upper row indicate the dendrite shapes shown in the three dimensions and the ones on the bottom row shown in 2-D section, respectively. The darkness of the figures in 2-D section indicates the concentration profiles in both the solid and liquid phases. Within the solid region, along the centerline of primary trunks or side arms, there exists a spine with lower concentration.

As the previously developed 2-D MCA model, the present 3-D MCA model also has significant advantages compared to the phase field models, such as the excellent computational efficiency and no cell size limitation. The computational time for Fig. 3 was only about 1.43 h on a Pentium III PC-1000 MHz. Whereas in the case of the phase field models, it should take about 6 h to calculate a very small 3-D primary trunk formation before emitting the side branch on 64 processors of the CRAY T3E at NerSC and use up to 5×10^6 walkers.[31]

4.2. Grain Selection in Directional Solidification

In order to investigate the mode of grain selection in directional solidification, the "pigtail" grain selector was used as shown in **Fig. 4**. The helix selector stands over a thin disk with a diameter of 500 μm and a thickness of 50 μm. The total cell number was 638 886 and the cell size was taken to be 5 μm. The selected grain number could be controlled by changing the helix diameter. Over the helix part, there is a cylinder letting the selected dendritic grains further grow. The selector connects the bottom disk over to a copper chill with a constant temperature of 298 K, whereas the other surfaces of the selectors are considered as almost

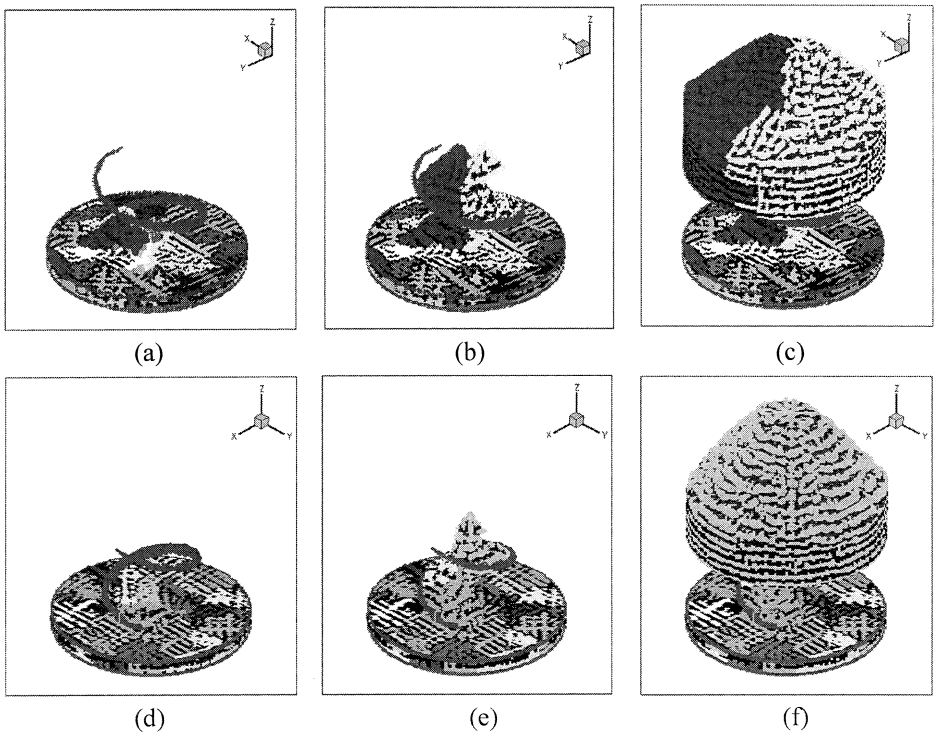

Fig. 4. Dendritic grain selection of an Al–4.5mass%Cu alloy in directional solidification: (a), (b) and (c) two grains selected; (d), (e) and (f) one grain selected.

Table 1. The nucleation parameters used in the present calculation.

	$n_{max,s}$ (m^{-2})	$\Delta T_{mn,s}$ (K)	$\Delta T_{\sigma,s}$ (K)	$n_{max,b}$ (m^{-3})	$\Delta T_{mn,b}$ (K)	$\Delta T_{\sigma,b}$ (K)
Fig. 4	1.2×10^{10}	0.5	0.1	4.0×10^{12}	5	0.1
Figs. 5,6	----	----	----	2.0×10^{13}	40	0.1

adiabatic. The heat transfer coefficient at the disk/chill interface and the superheat of melt were chosen to be 1 000 W/m^2 K and 30 K, respectively. In this simulation, the surface nucleation and bulk nucleation were only considered for the disk-chill surface and disk bulk, respectively. The nucleation parameters n_{max}, ΔT_{mn} and ΔT_{σ}, are listed in **Table 1**. The symbols indexed "s" and "b" are corresponding to nucleation parameters on the mold surface and in the bulk liquid, respectively.

Figure 4 shows the dendritic grain structures of an Al–4.5mass%Cu alloy solidified in the pigtail selectors. The different darkness of dendrite indicates its crystallographic orientation. It could be seen that many dendritic grains with different preferential growth orientations form on the bottom disk as shown in Figs. 4(a) and 4(d). Some of them enter the restrictive entry of the selector. As the dendrites competitively grow up in the helix part along the *Z*-axis, few dendritic grains could survive as shown in Figs. 4(b) and 4(e). In case of Fig. 4(c), two grains are selected. However, when the grain selector becomes narrow, as shown in Fig. 4(f), a single grain could form.

4.3. Dendritic Structures of Gas-atomized Al–Cu Alloy Droplets

The present model was also applied to predict the dendritic structure evolution of gas-atomized Al–10 mass%Cu alloy droplets under the non-uniform temperature field condition. The calculation domain consisted of 491 864 uniform cubic cells and the cell size was chosen to be 1 μm. The temperature of atmosphere was considered to be 298 K. The heat transfer coefficient at the droplet/air interface and the superheat of droplet were chosen to be 5 000 W/m^2 K and 30 K, respectively. The nucleation parameters used for the simulations are listed in Table 1.

Figure 5 indicates the sequences of microstructure evolution in an atomized Al–10mass%Cu droplet. The different darkness of each dendrite is an indication of its crystallographic orientation. The darkness of liquid indicates the concentration profile in the liquid phase. At the beginning stage of nucleation and dendrite growth, most crystals were normally nucleated in the vicinity of the surface due to the rapid heat extraction. It could be noted that as the nucleation and growth proceeds, the darkness of liquid near the S/L interface increases, which indicates that the liquid concentration in the region near the S/L interface increases owing to the solute redistribution during solidification. Finally, when all the regions completely solidified, the high concentration liquid within the dendrite arms became the eutectic phase.

The effect of the droplet size on microstructure was simulated by the present model and compared with the experiment results. **Figure 6** indicates the obtained microstructures with droplet sizes of (a) 40 μm, (b) 100 μm, and (c) 200 μm, which are shown in 2-D section. Figure 6(d) shows the three-dimensional outlook of dendritic morphology of a droplet with the diameter of 100 μm. The figures on the upper row indicate the predicted microstructures and on the bottom row the experimental ones. The different darkness represents the different crystallographic orientation of dendritic grains and the black color within the dendrite arms

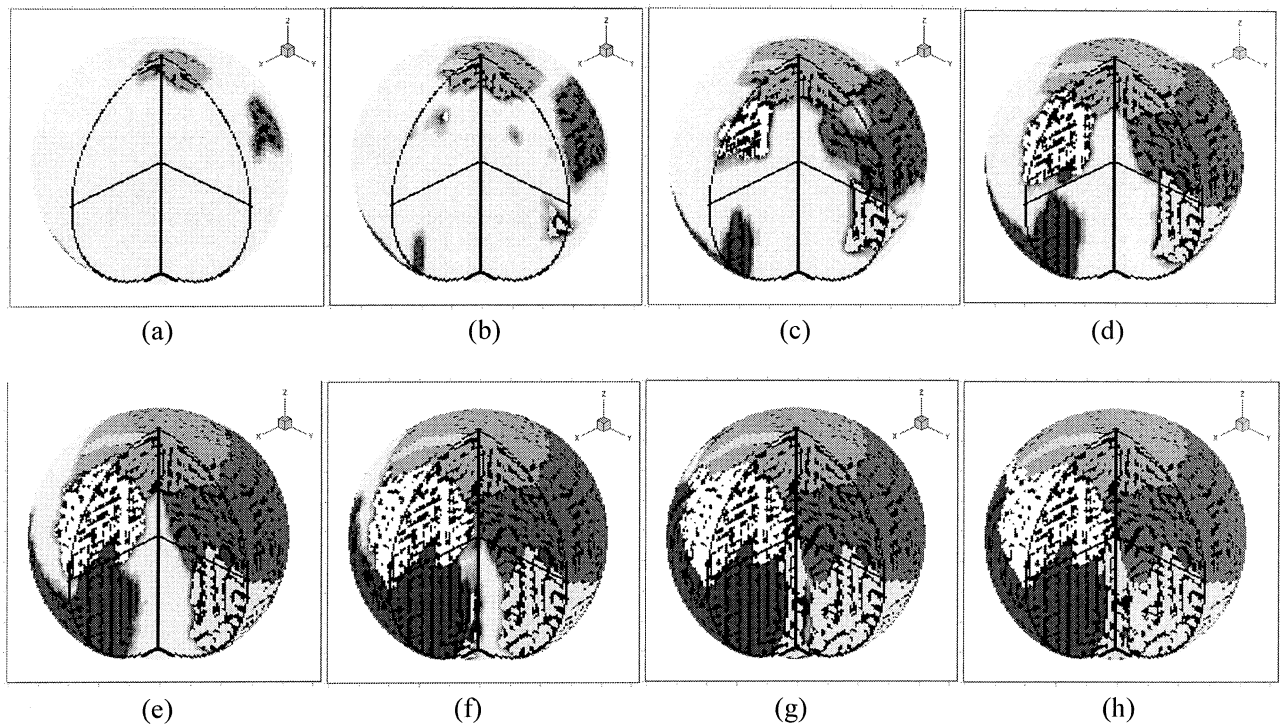

Fig. 5. The microstructure evolution of an atomized Al–10mass%Cu alloy droplet with for various solid fractions: (a) f_s=0.1, (b) f_s=0.2, (c) f_s=0.3, (d) f_s=0.4, (e) f_s=0.6, (f) f_s=0.7, (g) f_s=0.9, and (h) f_s=1.0.

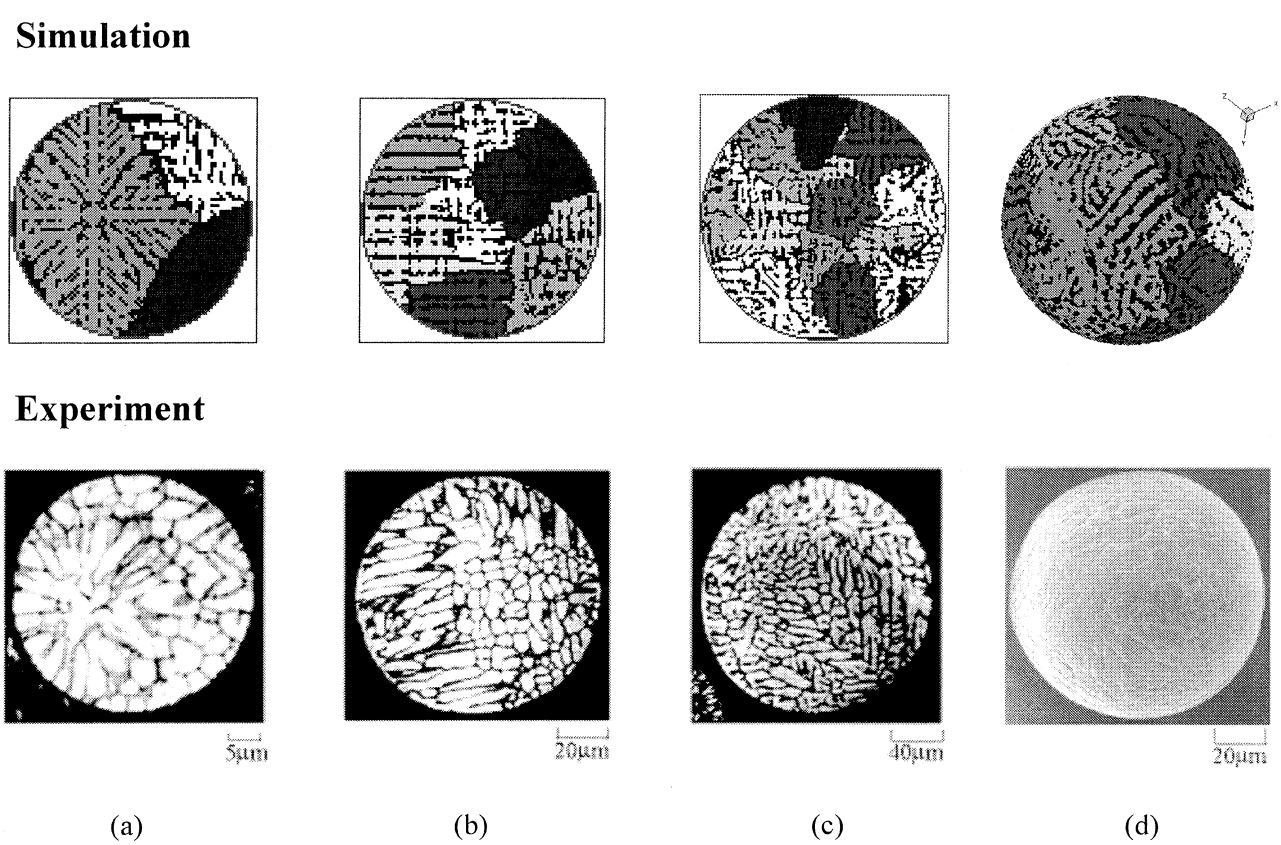

Fig. 6. Comparison between simulated and experimental microstructures of atomized Al–10mass%Cu droplets with various droplet sizes: (a) 40 μm, (b) 100 μm (c) 200 μm and (d) 100 μm. Here (a), (b) and (c) indicate the microstructures shown in 2-D cross section and (d) the three dimensional view of a droplet.

indicates the eutectic phase. It could be seen from the figures that as the droplet diameter increases from 40 to 200 μm, the number of dendritic grains in a droplet gradually increases. The figures also show that the present 3-D MCA model can predict not only the solidification grain structures, but also the dendritic morphology inside the

grains. The predicted microstructures are in good agreement with those obtained experimentally. The computational time for the calculations of Fig. 5 and Fig. 6 was about 20 to 25 min on a Pentium PC-1000 MHz.

5. Conclusion

A three-dimensional modified cellular automaton model has been developed in order to simulate the evolution of microstructures in solidification of alloys. The present 3-D MCA model includes the nucleation, growth kinetics, and the preferred growth orientation of a dendrite tip. It is also coupled with the curvature and solute redistribution both in liquid and solid phases during solidification. The free dendritic growth in three dimensions from an undercooled melt can be modeled by the present model with the excellent computational efficiency compared with the phase field models. The present 3-D MCA model can predict satisfactorily the multi-dendritic growth under the non-uniform temperature conditions, such as the dendritic grain selection in directional solidification and the dendritic microstructures of gas-atomized Al–Cu alloy droplets. It was found that as the previously developed 2-D MCA model, the 3-D MCA model can simulate not only the evolution of solidification grain structures, but also the detailed dendritic morphology inside the grains. Therefore, it can be concluded that the present 3-D MCA model can be used as a powerful tool to predict the microstructures in the practical castings. It is also expected that the simulated 3-D microstructures can be used as the valid information for the prediction of mechanical properties associated with microstructure features.

Acknowledgments

One of the authors (M. F. Zhu) is grateful to KOSEF (Korea Science and Engineering Foundation) for the financial support by a Brain Pool system. The authors would like to thank Dr. I. S. Cho for the helpful discussion. A part of this work was supported by the Brain Korea 21 Project.

REFERENCES

1) W. J. Boettinger, S. R. Coriell, A. L. Greer, A. Karma, W. Kurz, M. Rappaz and R. Trivedi: *Acta Mater.*, **48** (2000), 43.
2) D. M. Stefanescu: *ISIJ Int.*, **35** (1995), 637.
3) M. Rappaz and Ch.-A. Gandin: *Acta Metall. Mater.*, **41** (1993), No. 2, 345
4) Ch.-A. Gandin and M. Rappaz: *Acta Metall. Mater.*, **42** (1994), No. 7, 2233.
5) Ch.-A. Gandin, R. J. Schaefer and M. Rappaz: *Acta Mater.*, **44** (1996), No. 8, 3339.
6) S. G. R. Brown, N. B. Bruce: *J. Mater. Sci.*, **30** (1995), 1144.
7) K. Ravindran, S. G. R. Brown and J. A. Spittle: *Mater. Sci. Eng.*, **A269** (1999), 90.
8) I. S. Cho and C. P. Hong: *ISIJ Int.*, **37** (1997), 1098.
9) K. Y. Lee and C. P. Hong: *ISIJ Int*., **37** (1997), 38.
10) S. Y. Lee, S. M. Lee and C. P. Hong: *ISIJ Int*., **40** (2000), 48.
11) Y. H. Chang, S. M. Lee, K. Y. Lee and C. P. Hong: *ISIJ Int.*, **38** (1998), 63.
12) M. Rappaz, Ch.-A. Gandin, J.-L. Desbiolles and Ph. Thevoz: *Metall. Mater. Trans. A*, **27A** (1996), No. 3, 695.
13) Ch.-A. Gandin, M. Rappaz and R. Tintillier: *Metall. Mater. Trans. A*, **25A** (1994), No. 3, 629.
14) Ch.-A. Gandin and M. Rappaz: *Acta Mater.*, **45** (1997), No. 5, 2187.
15) Ch.-A. Gandin, J.-L. Desbiolles, M. Rappaz and Ph. Thevoz: *Metall. Mater. Trans. A*, **30A** (1999), No. 12, 3153.
16) A. Kermanpur, N. Varahram, P. Davami and M. Rappaz: *Metall. Mater. Trans. B*, **31B** (2000), No. 12, 1293.
17) M. F. Zhu and C. P. Hong: *ISIJ Int.*, **41** (2001), 436.
18) M. F. Zhu, J. M. Kim and C. P. Hong: *ISIJ Int.*, **41** (2001), 992.
19) S. L. Wang and R. F. Sekerka: *Phy. Rev. E*, **53** (1996), No. 4, 3760.
20) R. Kobayashi: *Physica D*, **63** (1993), 410.
21) S G. Kim, W. T. Kim, J. S. Lee, M. Ode and T. Suzuki: *ISIJ Int*., **39** (1999), 335.
22) J. A. Warren and W. J. Boettinger: *Acta Metall. Mater.*, **43** (1995), 689.
23) C. Beckermann, H.-J. Diepers, I. Steinbach, A. Karma and X. Tong: *J. Computational Phys.*, **154** (1999), 468.
24) J. A. Warren, R. Kobayashi and W. C. Carter: Modeling of Casting, Welding and Advanced Solidification Processes IX, ed. by P. R. Sahm, P. N. Hansen and J. G. Conley, Shaker Verlag Publishers, Aachen, (2000), Keynotes CII.
25) S. Wolfram: *Rev. Mod. Phys*., **55**, (1983), No. 3, 601.
26) Ph. Thevoz: Sc. Dr. Thesis No. 765, Swiss Federal Inst. Tech., Lausanne, (1988).
27) W. Kurz, B. Giovanola and R. Trivedi: *Acta Metall.*, **34** (1986), 823.
28) J. Lipton, W. Kurz and R. Trivedi: *Acta Metall.*, **35** (1987), 957.
29) G. X. Wang and E. F. Matthys: *Int. J. Rapid Solidif.*, **6** (1991), 141.
30) L. Nastac: Proc. Modeling of Casting and Solidification Processes IV, ed. by C. P. Hong, J. K. Choi and D. H. Kim, Hanrimwon, Seoul, (2000), 31.
31) A. Karma and M. Plapp: Proc. of Cutting Edge of Computer Simulation of Solidification and Casting, ed. by I. Ohnaka and H. Yasuda, ISIJ, Tokyo, (1999), 227.